Tailoring Double-Negative Metamaterial Responses to Achieve Anomalous Propagation Effects Along Microstrip Transmission Lines

Ching-Ying Cheng, *Member, IEEE,* and Richard W. Ziolkowski, *Fellow, IEEE*

***Abstract*—The design of a double-negative metamaterial loaded microstrip transmission line (DNG MTM-TL) to tailor the propagation characteristics at S- and C-band frequencies is presented. Guided-wave propagation along this DNG MTM-TL was studied numerically. The scattering parameters of the DNG MTM-TL were obtained with Ansoft's *High Frequency Structure Simulator*. A two-port network realization of the DNG MTM-TL is established. The effective permittivity and permeability for the DNG MTM-TL is extracted using this two-port network representation. It is shown that both a negative permittivity and a negative permeability and, hence, a negative index of refraction exist in the design frequency range. These material parameters are dispersive and conform to a two-time derivative Lorentz material model type of resonance behavior. This form of the index of refraction may be very suitable for applications dealing with phase and dispersion compensation along a microstrip transmission line.**

***Index Terms*—Artificial dielectrics, backward waves, dispersion, metamaterials (MTMs), propagation, transmission lines.**

I. Introduction

In RECENT years, there has been a renewed interest in using sub-wavelength structures to develop materials that mimic known material responses or that qualitatively have new response functions that do not occur in nature. These efforts include the realization of double-negative (DNG) materials, i.e., materials with both negative permittivity and negative permeability [1]–[4]. The transmission properties in such metamaterials (MTMs) have been studied by several groups, e.g., [5]–[10]. These MTMs are typically realized artificially as composite structures that are constructed from arrays of metallic inclusions in dielectric substrates. As discussed, e.g., in [11] and [12], they exhibit unusual scattering and propagation properties within a particular frequency range. For instance, in contrast to a double-positive (DPS) medium, i.e., a normal medium that has both positive permittivity and permeability, the wavenumber k in a DNG material is opposite to, rather that parallel to, the Poynting's vector associated with a plane wave propagating in it. Thus, the Poynting's vector is parallel to, and the wavenumber k is antiparallel to, the direction of causal power flow [5]. Fig. 1(a) shows the "right-handed" wave propagation behavior in a DPS medium and Fig. 1(b) shows the so-called "left-handed" wave propagation behavior in a DNG medium. Several experimental verifications of the existence of the DNG MTMs have been reported [13]–[15].

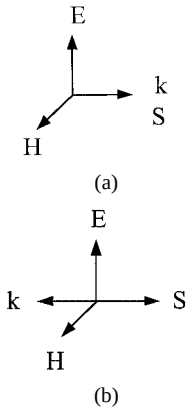

Fig. 1. Wave properties in: (a) DPS and (b) DNG mediums.

In this paper, we describe our study of the performance of microstrip transmission lines loaded with DNG MTMs formed by embedding capacitively loaded strips (CLSs) and capacitively loaded loops (CLLs) in the substrate region. It has been demonstrated numerically that a suitable arrangement of these components in Roger's 5880 Duroid $(\varepsilon_r = 2.2)$ produces a negative index of refraction in both the S-band (2–4 GHz) and C-band (4–8 GHz). This double-negative MTM loaded microstrip transmission line (DNG MTM-TL) problem will be reviewed in detail. Simulations of this complex guided-wave environment were performed with Ansoft's *High Frequency Structure Simulator* (*HFSS*). These results were used to characterize the S-parameter performance of this DNG MTM-TL configuration. It will be shown that a matched MTM can be obtained that yields complete transmission in both the S- and C-bands. Furthermore, it will be shown that a two-port network model can be used to extract the effective permittivity and permeability in that regime. Extracted values will be shown that yield DNG values in the matching region and, hence, that produce a negative index of refraction there. The corresponding group and phase velocities are also obtained. The property of interest to the microstrip transmission-line application involves the possibility that the wave impedance in the DNG MTM could be matched to the intrinsic impedance of the transmission line and, due to their dispersive nature, can then be used to achieve nonstandard propagation characteristics along it.

Manuscript received March 28, 2003. This work was supported in part by the Intel Corporation.

The authors are with the Department of Electrical and Computer Engineering, University of Arizona, Tucson, AZ 85721-0104 USA (e-mail: ccheng@ece.arizona.edu; ziolkowski@ece.arizona.edu).

Digital Object Identifier 10.1109/TMTT.2003.819193

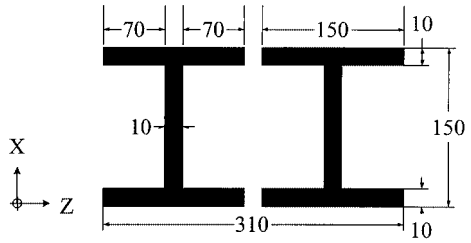

Fig. 2. CLS unit cell (units = mil).

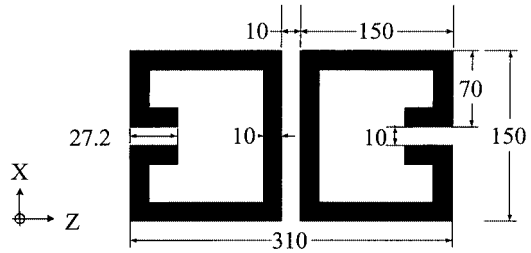

Fig. 3. CLL unit cell (units = mil).

Potential applications to modify the shape of signals propagating along these DNG MTM-TLs will be discussed briefly.

II. MTM Design

The DNG MTM components are derived from those successfully tested in [15]. There, an integrated set of negative permittivity (CLS) and negative permeability [split ring resonator (SRR)] elements were used to obtain a negative index of a refraction block that was matched to free space at the X-band. The MTM elements considered here consist of a pair of CLSs and a pair of oppositely oriented CLLs. These CLLs behave similarly to the SRRs, but greatly simplify fabrication issues. These elements are embedded in a lossless dielectric characterized by the parameters $\varepsilon_r = 2.2$ and $\mu_r = 1.0$ corresponding to Roger's 5880 Duroid material. The basic CLS and CLL unit cells are shown in Figs. 2 and 3, respectively. Both unit cells have a total height (distance orthogonal to the ground plane) of 160 mil (1.0 mil $= 0.001$ in $= 25.4\,\mu$m) and a depth of 310 mil. The height of both the CLS and CLL elements was 150 mil, leaving a 5.0-mil gap between the tops and bottoms of these elements and the ground plane and microstrip trace. The sizes of the CLSs and CLLs were determined to provide interesting responses in the 3–5-GHz frequency regime. These results could be scaled to higher or lower frequencies based upon the size of these elements.

The electric field of the microstrip transmission line is incident parallel to the strips along the x-axis and the corresponding magnetic field is normal to the loops along the x-axis. The direction of propagation is along the z-axis; the direction of the capacitor legs coincides with the z-axis. The CLLs in each pair are oppositely oriented to create a MTM element that, like the CLS pair, is reciprocal for a wave propagating from the positive or negative z-directions. The top view of the integrated DNG MTM block is shown in Fig. 4. The DNG MTM block contains one CLL unit cell and two CLS unit cells with a 10-mil spacing between them. In addition, a 5-mil spacing is used between each CLS pair and the outer y edges of the block. Therefore, the dimensions of a unit DNG MTM block are 150 mil × 30 mil × 310 mil.

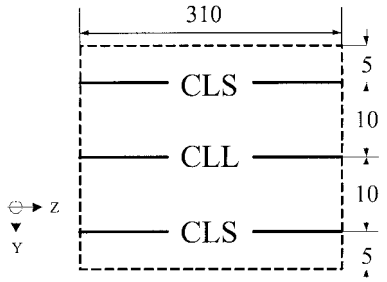

Fig. 4. Top view of the unit MTM block (units = mil).

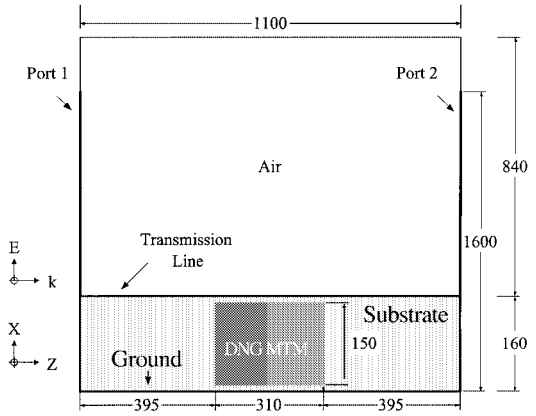

Fig. 5. Side view of the designed MTM-loaded TL (units = mil).

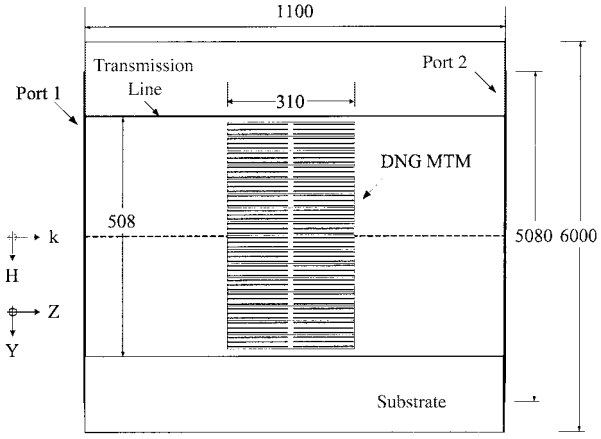

Fig. 6. Top view of the designed MTM-loaded TL (units = mil).

III. *HFSS* Simulation Results

A. Simulation Setup

To tailor the DNG responses along a microstrip transmission line using *HFSS*, the geometry shown in Figs. 5 and 6 was created. It led to the simulation space shown in Fig. 7 whose size was 2000 mil × 6000 mil × 1100 mil. A 50-Ω microstrip transmission line was designed whose trace width and length were, respectively, 508 and 1100 mil for the assumed height of 160 mil of the substrate ($\varepsilon_r = 2.2$ and $\mu_r = 1.0$). Since the y-width of a single DNG MTM block was 30 mil, this allowed a total of 16

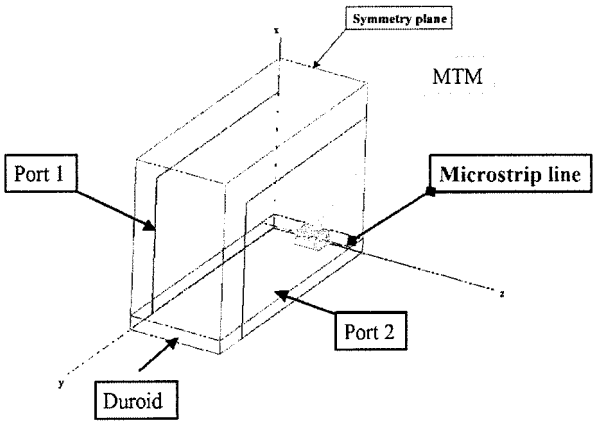

Fig. 7. Three-dimensional view of the *HFSS* setup for the MTM-loaded TL simulations.

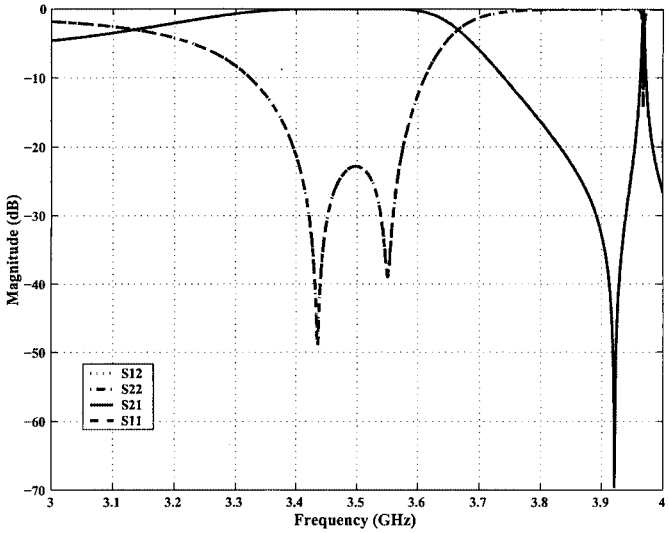

Fig. 8. Magnitudes of the normalized and deembedded S-parameters.

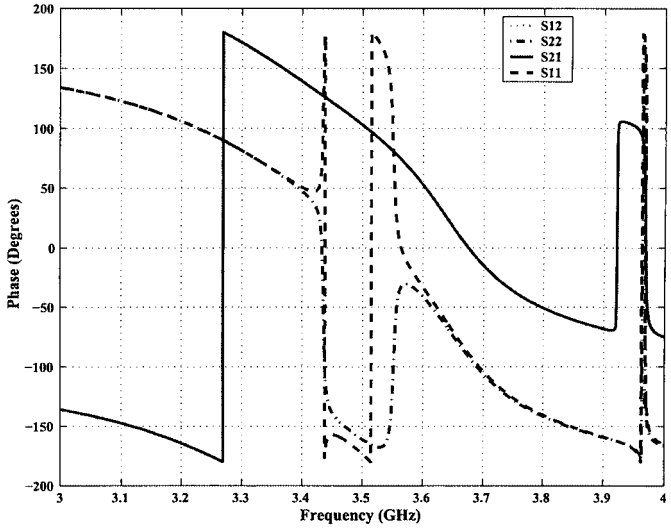

Fig. 9. Phases of the normalized and deembedded S-parameters.

DNG MTM blocks to be placed under the transmission line. The DNG MTM blocks were aligned to be in the center of the geometry (dotted line in Fig. 6). Therefore, there were 14 mil of space from both edges of the transmission line that did not have DNG MTM under it. The trace length over the DNG MTM block coincided with its length of 310 mil. The entire set of DNG MTM blocks was placed 395 mil from both ports. Thus, the input and output transmission-line lengths were also 395 mil. This distance was sufficient to prevent coupling between any evanescent waves from the edges of the DNG MTM region and ports.

Ports were placed at both z-boundaries. It is important to point out that the size of each port was selected to be large enough to obtain accurate results in *HFSS*. In particular, the size of the ports were set to 1600 mil in height and 5080 mil in width, i.e., 10$\times$ larger than the transmission line height and width. A port impedance line was applied to define the voltage at the port and a port calibration line was applied to remove a possible 180° phase ambiguity. Thus, consistent phases for S_{21} and S_{12} were obtained. The S-parameter results were finally deembedded 395 mil from each port to the front and back faces of the DNG MTM block.

The transmission line, ground plane, CLSs, and CLLs were assumed to be perfect conductors. Air was assumed to be present above the substrate. Radiation boundaries were used on the $\max$-x-, $\max$-y-, $\min$-z-, and $\max$-y-planes. Due to the symmetry of the problem, a vertical symmetry H-plane was inserted on the $\min$-y-plane shown in Fig. 6. Consequently, only half of the DNG MTM-TL structure was actually simulated. The number of tetrahedral required to achieve the ΔS convergence criterion of 0.001 was 99 603. A 10-GHz single frequency was used to established the mesh. The frequency behavior associated with the simulation was obtained as a fast sweep to obtain 5000 frequency points from 2 to 5 GHz.

B. HFSS Calculated DNG MTM-TL Results

Due to the guided wave nature of the source, the S-parameters were normalized to remove any dependencies on the impedance of the input/output microstrip lines. The 2×2 scattering S-matrix was obtained from *HFSS* for the entire structure for the indicated set of frequencies. The results were then deembedded to the surfaces of the DNG MTM block. The characteristic impedance of each port at every frequency point was obtained and used to construct the normalized S-matrix. Due to the size of the MTM block and overall guiding structure, as well as the complicated shape of the scatterers (i.e., the inclusions), higher order propagating and evanescent modes may be present. All modes were taken into account in the *HFSS* simulations.

The resulting deembedded and normalized magnitudes and phases of the *HFSS* predicted S_{11}, S_{12}, S_{21}, and S_{22} values for the DNG MTM-TL structure are shown in Figs. 8 and 9 from 3 to 4 GHz. A complete passband exists in the frequency region of 3.3–3.6 GHz. The overall phase of S_{21} passes through 90° in the middle of this band at 3.53 GHz. Removing either of the CLS or the CLL elements caused a stopband in this frequency region. This behavior was analogous to that observed in the free-space DNG modeling and experiments [15]. Consequently, we claim that the DNG MTM blocks are acting as a DNG medium in this frequency region.

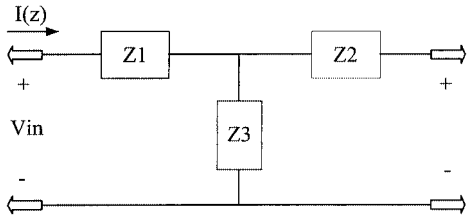

Fig. 10. Two-port T-network representation of the DNG MTM-TL.

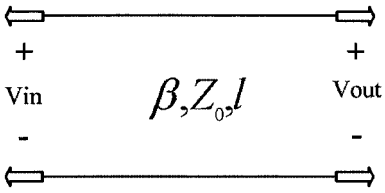

Fig. 11. Two-port network representation of the DNG MTM-TL.

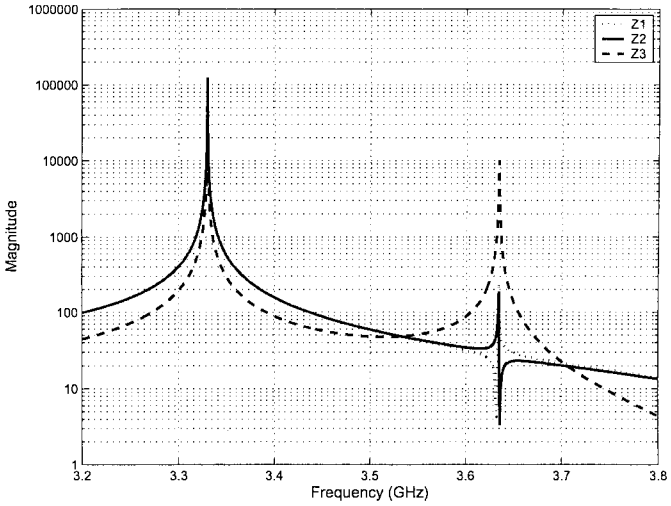

Fig. 12. Extracted magnitudes of the impedances.

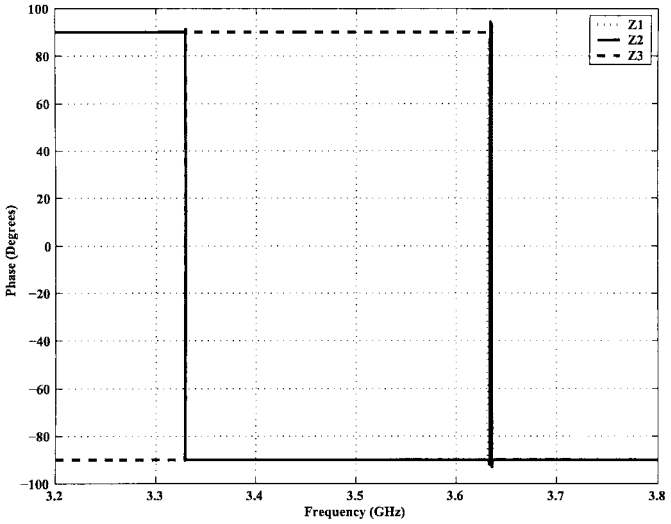

Fig. 13. Extracted phases of the impedances.

IV. Extraction of the Effective Material Properties

To substantiate this claim, we utilize a two-port network approach to extract the effective material parameters of the DNG MTM-TL and to study the wave propagation behavior along it. There are many potential choices. For example, one possible two-port network representation of the MTM loaded transmission-line section is the T-network set of impedances (Z_1, Z_2, and Z_3) shown in Fig. 10. Another choice is the lossless transmission line of length l representation shown in Fig. 11. It will be shown that both provide complementary, but consistent information about the effective medium behavior of the DNG MTM-TL.

A. Extracted Properties Using the T-Network Representation

To extract the effective material properties using a T-network set of impedances, the deembedded and normalized S-parameters were connected to the equivalent $ABCD$ matrix via the standard expressions [16]. The resulting $ABCD$ matrix was used to calculate the impedances Z_1, Z_2, and Z_3 of the two-port network with the expressions

$$Z_1 = \frac{A-1}{C}$$
$$Z_2 = \frac{D-1}{C}$$
$$Z_3 = \frac{1}{C}. \tag{1}$$

The magnitudes and phases of the impedances Z_1 (dotted line), Z_2 (solid line), and Z_3 (dashed line) are shown in Figs. 12 and 13, respectively.

It was found that the extracted impedances had large variations in their amplitudes across the frequency range. However, the impedances Z_1, Z_2, and Z_3 varied dramatically at the edges of the passband. From the extracted phases, one can see that the DNG MTM loaded transmission line can be represented as a normal *L–C* transmission line before the DNG passband. It switches to a *C–L* configuration in the DNG passband. It then switches to a *C–C* type of configuration after the DNG passband where complete reflectivity ($|S_{11}| \sim 1$) is exhibited. This *C–L* type of behavior has been shown in [14] to be characteristic of a planar DNG transmission line. As expected, it was found that propagating waves in the MTM block would exist only if both the *L* and *C* element characteristics were present.

It was also found that the impedance at the frequency 3.53 GHz is 50 Ω and $A = 0$. From the $ABCD$ matrix representation this means $B \approx -Z_0\ S_{12}$. The equivalent transmission line $ABCD$ matrix (see (2) below) then yields $B = jZ_0 \sin\beta l \approx -Z_0 S_{12} = -jZ_0$ at this point. Since $\beta l = n(2\pi l/\lambda)$, this means $n < 0$ at this point and $|n| = (m + 1/4)\lambda/l$ or, alternatively, $n > 0$ and $|n| = (m + 3/4)\lambda/l$. Expecting the lowest order result to dominate, this result would indicate that the index of refraction is negative, i.e., $n = -2.69$ at this point. Further considerations summarized in Section IV-B show that negative values of the index occur within the DNG passband at frequencies surrounding this point. This corresponds to the results shown in [5], i.e., the CLS-CLL DNG MTM design creates an effective medium that has a negative index of refraction.

B. Extracted Properties Using the Lossless Transmission-Line Representation

The extraction method associated with the T-network representation illustrated in Section IV-A assumes that Z_1, Z_2, and Z_3 are independent of each other, i.e., that there is no coupling between the impedance elements. This would not necessarily be the best representation for the DNG MTM-TL structure shown in Fig. 5 since that structure tightly integrates the CLS and CLL elements into the unit cell. We feel that near the passband frequency region of the DNG MTM-TL, the two-port network representation of a lossless transmission line of length l given in Fig. 11 may be suitable. It reflects the reciprocal and symmetric properties of the DNG MTM-TL under consideration.

The $ABCD$ matrix of a two-port network representation of a lossless transmission line has the following form:

$$\begin{pmatrix} A & B \\ C & D \end{pmatrix} = \begin{pmatrix} \cos\beta l & jZ_0 \sin\beta l \\ jY_0 \sin\beta l & \cos\beta l \end{pmatrix} \tag{2}$$

where β and $Z_0(f)$ are, respectively, the characteristic wavenumber and impedance of the transmission line and $Y_0(f) = 1/Z_0(f)$ is its characteristic admittance. Inserting these expressions into the $ABCD$ matrix elements, one can solve for the effective material properties as follows.

1) Extracted Permittivity and Permeability: Recall that the propagation constant and the impedance are given by the expressions

$$\begin{aligned} \beta &= \omega\sqrt{\varepsilon\mu} \\ Z_0 &= \sqrt{\frac{\mu}{\varepsilon}}. \end{aligned} \tag{3}$$

Assuming that l/λ is small, the relative permeability (μ_r) can then be extracted from (2) and the $ABCD$ matrix elements can then be extracted by calculating the expression

$$\frac{B}{A} = \frac{jZ_0 \sin\beta l}{\cos\beta l} = jZ_0 \tan\beta l \cong jZ_0\beta l. \tag{4}$$

By combining (3) and (4), one then obtains

$$\mu_r = \frac{B}{j\omega\mu_0 lA}. \tag{5}$$

Similarly, the relative permittivity (ε_r) can be extracted by first calculating the expression

$$\frac{C}{A} = \frac{jY_0 \sin\beta l}{\cos\beta l} = jY_0 \tan\beta l \cong jY_0\beta l. \tag{6}$$

By combining (6) and (3), one then obtains

$$\varepsilon_r = \frac{C}{j\omega\varepsilon_0 lA}. \tag{7}$$

The values of the real and imaginary parts of μ_r were obtained from (5) and are plotted in Fig. 14. A two-time derivative Lorentz (2TDLM) material [15] type of resonant behavior appears to be present near 3.52965 GHz. The amplitude of the real and imaginary parts of μ_r were both negative just above this resonant frequency. The amplitude of the real part of the relative permeability $\mu_r(\mu_{r,r})$ reached its most positive value, i.e., 280.96, at 3.5296 GHz, passed through zero at 3.52965 GHz, and then reached its most negative value, i.e., −281.22, at 3.5297 GHz. The amplitude of the imaginary part of the relative permeability $\mu_r(\mu_{r,i})$, which is negative everywhere, reached its most negative value, i.e., −308.74, at 3.5297 GHz.

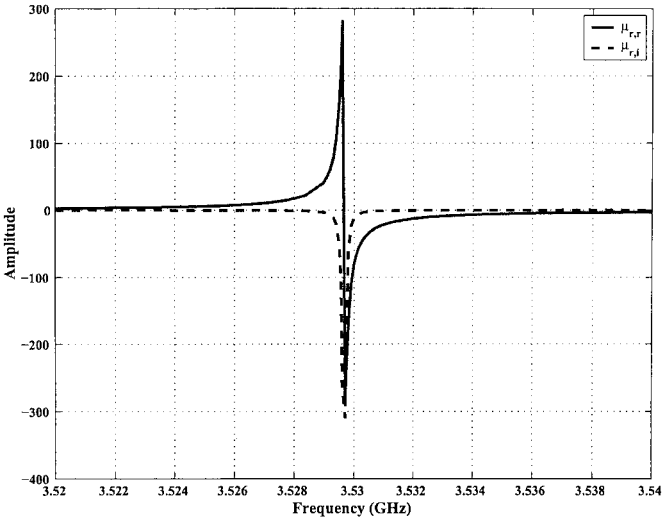

Fig. 14. Extracted relative permeability.

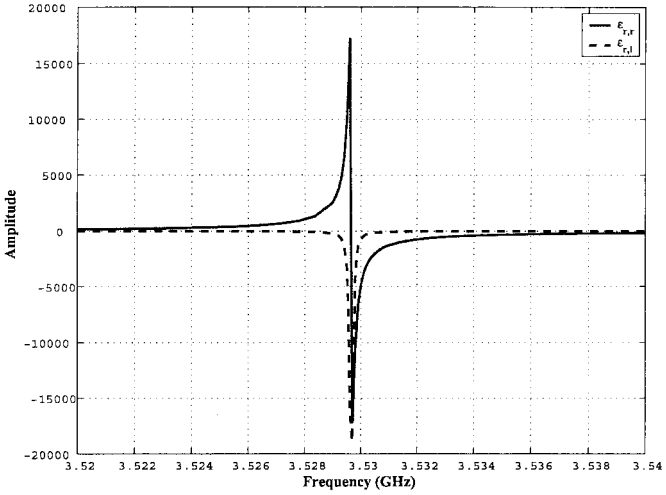

Fig. 15. Extracted relative permittivity.

In a similar manner, the real and imaginary parts of the resulting ε_r were obtained with (7) and are plotted in Fig. 15. Here, we find that a 2TDLM material type of resonant behavior is superimposed on a background Drude behavior near 3.52965 GHz. The amplitude of the real and imaginary parts of ε_r were also both negative just above this resonant frequency. The amplitude of the real part of the relative permittivity $\varepsilon_r(\varepsilon_{r,r})$ reached its most positive value, i.e., 17177, at 3.5296 GHz, passed through zero at 3.52965 GHz, and then reached its most negative value, i.e., −17160, at 3.5297 GHz. The amplitude of the imaginary part of the relative permittivity $\varepsilon_r(\varepsilon_{r,i})$, which is also always negative, reached its most negative value, i.e., −18870, at 3.5297 GHz. We note that these

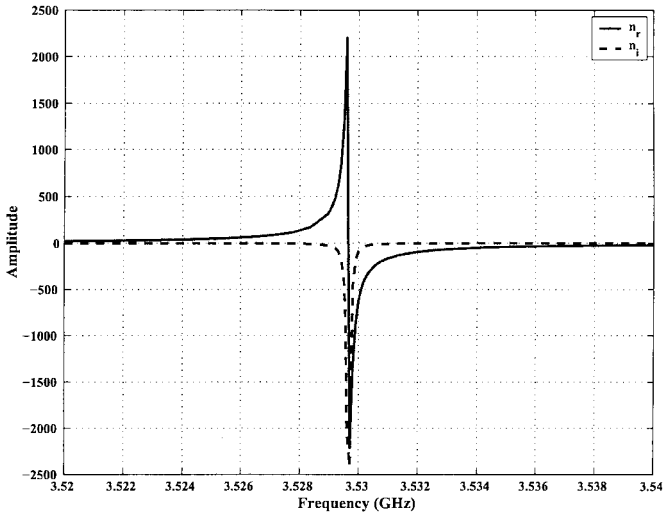

Fig. 16. Extracted index of refraction.

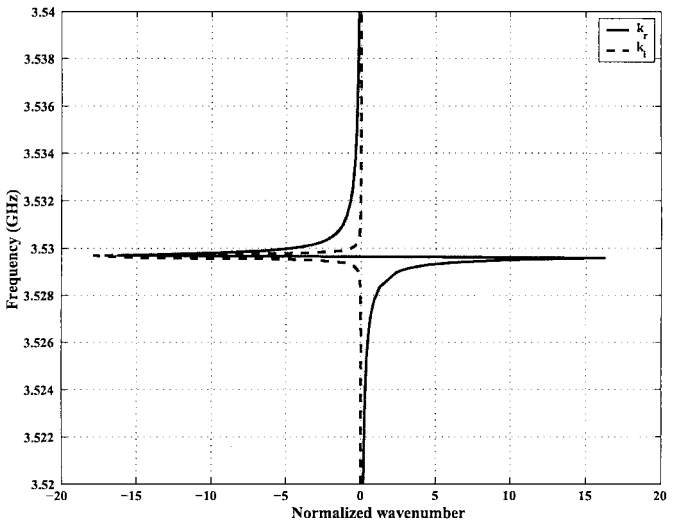

Fig. 17. $\omega - \beta$ diagram for the two-port network of the DNG MTM TL. The amplitude of the wavenumber is normalized to 10 000.

extremely large values of the extracted material parameters are due to the resonant nature of the response and to the assumption that each component is lossless. Losses that are present in any realization of the DNG MTM-TL will significantly broaden the resonance and correspondingly decrease these amplitudes.

As mentioned in [15], it was expected that the CLSs would produce the main contribution to the electric susceptibility response and the CLLs should produce the main contribution to the magnetic susceptibility response. We note that, from Figs. 14 and 15, the amplitude of the real and imaginary parts of ε_r were much greater than the amplitude of the real and imaginary parts of μ_r and, hence, the CLSs appear to have provided a stronger effect than the CLLs did.

2) Extracted Index of Refraction: The index of refraction of the MTM block can be obtained immediately from the extracted values of ϵ_r and μ_r as

$$n(\omega) = \sqrt{\varepsilon_r}\sqrt{\mu_r}. \tag{8}$$

The real (n_r) and imaginary (n_i) parts of the index of refraction calculated with (8) are plotted in Fig. 16. Similar to Figs. 14 and 15, a predominant 2TDLM material type of resonant behavior is present near 3.52965 GHz. Away from the resonance, the behavior is a mixture of the 2TDLM and Drude responses. The amplitude of the real and imaginary parts of n were both negative just above this resonant frequency. The amplitude of n_r reached its most positive value, i.e., 2196.84, at 3.5296 GHz, passed through zero at 3.52965 GHz, and then reached its most negative value, i.e., -2196.78, at 3.5297 GHz. The amplitude of n_i reached its most negative value, i.e., -2413.63, at 3.5297 GHz. Since each of the CLS and CLL elements provides a contribution to the electric and magnetic susceptibility responses near their resonant frequencies, the effective permittivity and permeability of the complete DNG MTM were affected by the combined effects of both CLS and SRR structures together. Indeed, from Figs. 14–16, the designed DNG MTM-TL exhibited negative permittivity, negative permeability, and negative index of refraction in the frequency region of interest.

We note that while the conduction losses in the metals were assumed to be zero, the presence of the nonzero n_i values at the resonance frequency corresponds to the local storage of electromagnetic energy in the MTM block. In related time-domain calculations [15], it was found that the analogous free-space matched DNG MTM radiated this stored energy long after the excitation signal passed through it.

3) Extracted $\omega - \beta$ Diagram: Now consider the wave propagation behavior along the DNG MTM-TL. A quasi-TEM plane wave propagating in the $+z$-direction can be represented as

$$\vec{E} = E_0 e^{-j\beta z}\hat{x} \tag{9}$$

$$\vec{H} = \frac{E_0}{Z} e^{-j\beta z}\hat{y}. \tag{10}$$

The corresponding time-averaged Poynting's vector is

$$\langle \vec{S}_\omega \rangle = E_x \times H_y^* = \frac{|E_0|^2}{Z}\hat{z}. \tag{11}$$

The wave impedance $Z = \sqrt{\mu_r/\epsilon_r}Z_0$; the propagation constant β has the form

$$\beta = \omega\sqrt{\varepsilon}\sqrt{\mu} = \frac{\omega}{\sqrt{\varepsilon_0}\sqrt{\mu_0}}\sqrt{\varepsilon_r}\sqrt{\mu_r} = \frac{\omega}{c}n(\omega) \tag{12}$$

where c is the speed of light. The phase and group velocities are expressed in their well-known forms

$$v_p = \frac{\omega}{\beta} = \frac{c}{n(\omega)} \tag{13}$$

$$v_g = \left(\frac{\partial\beta}{\partial\omega}\right)^{-1}. \tag{14}$$

The dispersion diagram of the DNG MTM-TL was obtained from (12) and is plotted in Fig. 17.

Starting from 3.51 GHz in Fig. 17, the wavenumber β increases rapidly and reaches its maximum value $+162\,400\ m^{-1}$ at 3.5296 GHz. The wavenumber then decreases just as rapidly, passing through zero at 3.52965 GHz. It reaches its minimum value $-162\,400\ m^{-1}$ at 3.5297 GHz. Moreover, starting from 3.5297 GHz, the wavenumber again increases rapidly and goes to zero at 3.6937 GHz. We note that the value $\beta_{\max} l \sim 1279$

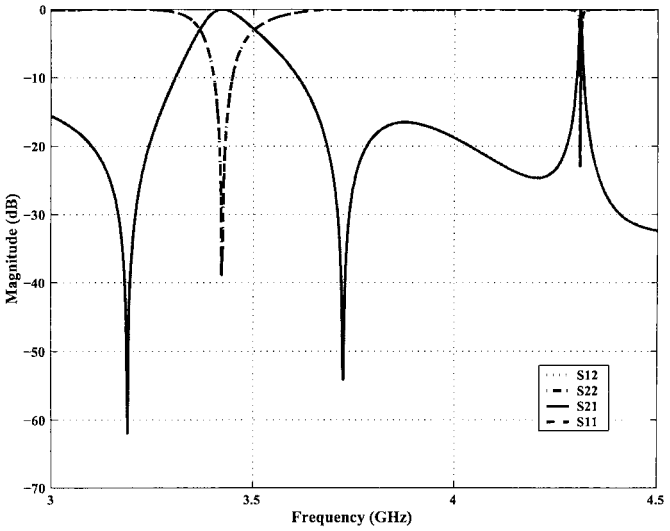

Fig. 18. Magnitudes of the normalized and deembedded S-parameters.

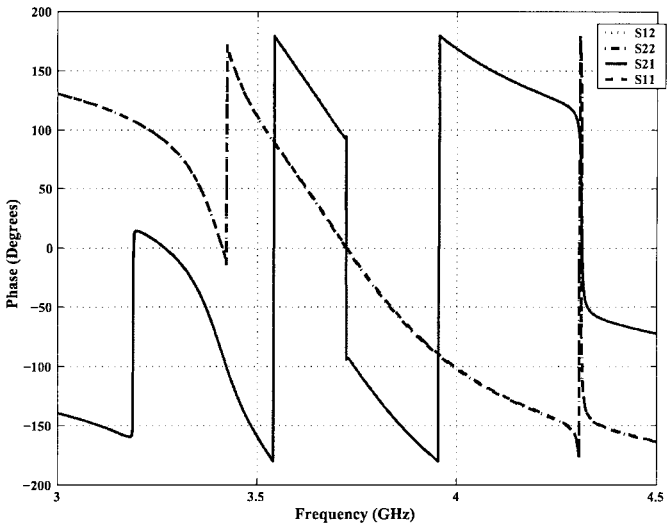

Fig. 19. Phases of the normalized and deembedded S-parameters.

is not small, while $l/\lambda = 0.093$ is small. We find that $|\beta l| < 1$ when $f < 3.41$ GHz and $f > 3.6$ GHz. Thus, the approximation we used to derive the index of refraction is not very accurate in the immediate vicinity of the resonance. Consequently, the maximum and minimum values of the extracted parameters are not precise. Nonetheless, the product $\beta_{\max} l$ quickly becomes small away from the resonance region and the approximate results are valid there. Thus, the 2TDLM shape of the ε_r, μ_r, and n_r curves near the resonance and their signs are believed to be correct. Moreover, this behavior is also consistent with the T-network representation results.

Clearly, in the frequency range of 3.51–3.52965 GHz, both the phase and group velocities are positive. The phase velocity v_p is positive, corresponding to the fact that the propagation constant β and the real part of the index of refraction n_r are positive as well. Therefore, the wavenumber has the same direction as the Poynting's vector. This wave propagation behavior is characteristic of a conventional transmission line residing over a normal DPS medium where v_p, v_g, and $\langle \vec{S}_\omega \rangle$ all have the same direction as shown previously in Fig. 1(a). In contrast, in the frequency range 3.52965–3.6937 GHz, the phase velocity is negative and the group velocity is positive. The fact that v_p is negative corresponds to negative values for both the propagation constant β and the real part of the index of refraction n_r. Therefore, the wavenumber has a direction opposite to that of $\langle \vec{S}_\omega \rangle$. This behavior was depicted previously in Fig. 1(b). This type of backward wave behavior has also been reported in [14], [17], and [18]. Notice that the DPS and DNG regions are interchanged around 3.52965 GHz where the resulting propagation constant β passes through zero.

C. Dual MTM Design

We also modeled the "dual" case in which the CLSs and the CLLs were interchanged, i.e., there were two pairs of CLLs and only one pair of CLSs in the unit cell. It was expected that the magnetic susceptibility would increase its amplitude in this case. The magnitudes and phases of the *HFSS*-predicted S-parameter results are shown, respectively, in Figs. 18 and 19. The magnitude of the transmission coefficient becomes unity,

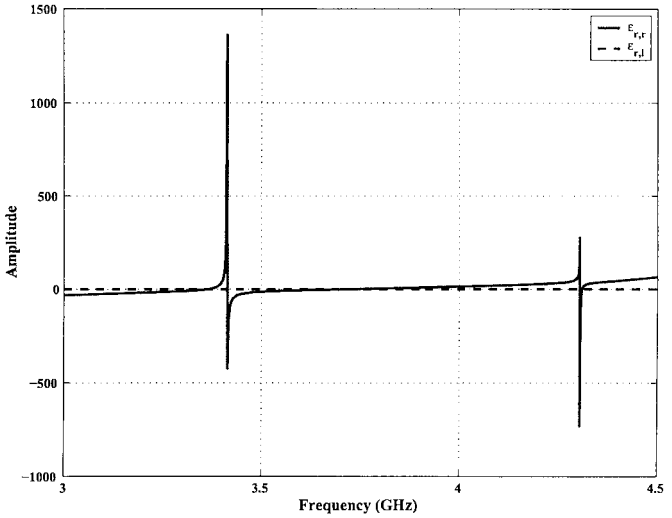

Fig. 20. Extracted relative permittivity.

i.e., $S_{21} = 1$ at 3.422 and 4.31 GHz. The effective permittivity and permeability were extracted using the lossless transmission-line method. The results are shown, respectively, in Figs. 20 and 21. Resonances in the permittivity occur at 3.4135 and 4.3053 GHz; resonances in the permeability occur at 3.4135, 3.723, and 4.3053 GHz. The frequencies at which the transmission coefficient becomes one corresponds to the frequencies where the permittivity and the permeability are both resonant. Total reflection occurred where only the permeability was resonant and, hence, where very large impedance values were exhibited by the MTM block. In fact, one finds that $S_{11} = 1$ and $\Phi_{S11} = 0$ at 3.723 GHz; this means that the MTM block acts as a perfect magnetic conductor (PMC) at that frequency.

These results are considerably different from those obtained with the original configuration. The S-parameters, particularly the phases, have a smoother behavior. The fact that the permeability is strongly impacted by the CLLs is demonstrated by the presence of the third resonance at 3.723 GHz while there is not one present in the permittivity.

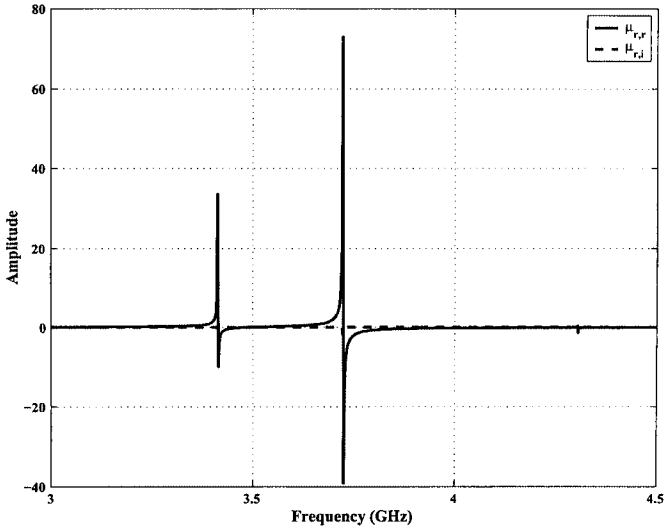

Fig. 21. Extracted relative permeability.

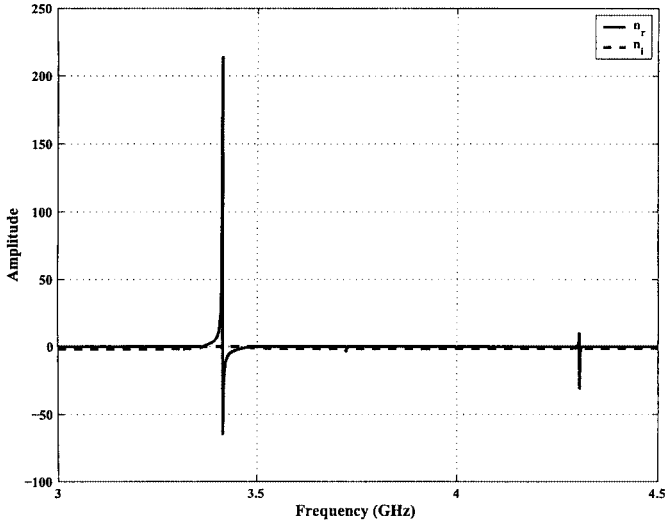

Fig. 22. Extracted index of refraction.

We believe that the differences between the configurations is a result of the fact that although the CLSs are dominated by electric-field effects and the CLLs are dominated by magnetic-field effects, a CLS pair forms a loop with two capacitors. Thus, the CLSs also have nontrivial magnetic-field contributions. On the other hand, since the CLLs are oriented in opposite directions, their electric-field effects are mitigated at certain frequencies. Thus, while a strong effect on the magnetic fields is still present and is expressed in the permeability, there is little effect on the permittivity. The presence of the third resonance in the permeability and its absence in the permittivity is a direct result of this behavior. Consequently, one observes that the presence of more CLSs or CLLs provides more possible couplings between the individual elements responsible for the effective permittivity and permeability and, hence, the opportunity for more complicated behaviors in the composite structure.

The extracted index of refraction is shown in Fig. 22. Large resonant responses occur at 3.4135 and 4.3053 GHz. The peak values of the real part of the index are explicitly $n_r = 214.0$ at 3.412 GHz and -65.0 at 3.414 GHz; and $n_r = 10$ at 4.305 GHz and -31.0 at 4.306 GHz. The imaginary part of the index $n_i = -1.0$ at 3.412 GHz and $n_i = -0.25$ at 4.306 GHz. Thus, one finds that the dual MTM block exhibits very low-loss unity transmission with a negative index of refraction just above these resonance frequencies.

Comparing the dual and original configuration results, we are led to the conclusion that the behaviors of the CLSs and CLLs are very tightly coupled together. Consequently, the complete response of the MTM block can only be evaluated with both species present in a self-consistent calculation such as those provided by *HFSS*.

D. Potential Applications

The ability to load a transmission line with DNG MTM-TL segments suggests the possibility of phase compensation through the associated negative index of refraction. Dispersion compensation may also be possible since this negative index of refraction is frequency dependent. These DNG MTM-TL segments may provide a means to achieve a self-annealing signal propagation environment by carefully designing the passband characteristics to compensate for the known dispersive nature of the microstrip line.

We note that because the DNG MTM-TL elements are highly resonant, their frequency-domain properties have rather narrow bandwidths. For instance, preliminary calculations of pulses propagated along the DNG MTM-TLs presented here, i.e., obtaining the output pulse as the inverse Fourier transform of the product of the input pulse's frequency spectrum and the DNG MTM-TLs frequency-domain transfer function $S_{21}(f)$, show expected narrow-bandwidth filtering behaviors. Nonetheless, it is anticipated that by serially staging several DNG MTM blocks whose reflection and transmission properties have slightly shifted frequency behaviors, one would be able to design a broad-bandwidth pulse-shaping device. This application is currently under investigation.

We also note that the MTM blocks considered here were designed specifically for straight transmission-line sections. Since these MTM constructs are very anisotropic, they could not necessarily be used directly in bends or junctions. Modified MTM designs would most likely be needed and could be tailored to a specified discontinuity and its application.

V. Conclusions

A DNG MTM loaded transmission line has been designed and its propagation characteristics have been presented. The MTM CLS and CLL elements used successfully in previous DNG MTM experiments have been modified and placed under a section of a microstrip transmission line. The resulting DNG MTM-TL structure has been simulated with *HFSS* and the effective material parameters have been extracted by using an equivalent two-port network approach. It was demonstrated that the DNG MTM-TL is characterized by a negative permittivity, negative permeability, and negative index of refraction in a particular frequency band. A 2TDLM material type of resonant frequency behavior of those material parameters was realized in that region. It was also shown that this region corresponds to a backward propagating wave region characterized by a negative phase velocity and positive group velocity.

Phase and dispersion compensating transmission-line segments formed by the DNG MTM-TLs have several potential applications. Issues including reduced dispersion behavior of signal pulses propagating along composite DNG MTM TLs and potentially reduced crosstalk effects between parallel DNG MTM TLs due to the self-focusing in the DNG MTM regions are currently under investigation. Experiments to validate the analysis and numerical simulations presented here are also under consideration. The results of these continuing efforts will be reported in the near future.

ACKNOWLEDGMENT

The authors would like to thank the Intel Corporation for their kind support. Several of the calculations performed were enabled by the generous donation of a Dell 530 Workstation by the Intel Corporation.

REFERENCES

[1] V. G. Veselago, "Electrodynamics of substances with simultaneously negative electrical and magnetic permeabilities," *Sov. Phys.—Usp.*, vol. 10, pp. 5–13, Jan.–Feb. 1968.

[2] J. B. Pendry, "Negative refraction makes a perfect lens," *Phys. Rev. Lett.*, vol. 85, no. 18, pp. 3966–3969, Oct. 2000.

[3] D. R. Smith and N. Kroll, "Negative refractive index in left-handed materials," *Phys. Rev. Lett.*, vol. 85, no. 14, pp. 2933–2936, Oct. 2000.

[4] R. Ruppin, "Extinction properties of a sphere with negative permittivity and permeability," *Solid State Commun.*, vol. 116, pp. 411–415, 2000.

[5] R. W. Ziolkowski and E. Heyman, "Wave propagation in media having negative permittivity and permeability," *Phys. Rev. Lett.*, vol. 64, pp. 056 625/1–056 625/15, Nov. 2000.

[6] R. A. Shelby, D. R. Smith, S. C. Nemat-Nasser, and S. Schulta, "Microwave transmission through a two-dimensional, isotropic, left-handed metamaterial," *App. Phys. Lett.*, vol. 78, no. 4, pp. 489–491, Jan. 2001.

[7] R. W. Ziolkowski, "Superluminal transmission of information through an electromagnetic metamaterial," *Phys. Rev. E, Stat. Phys. Plasmas Fluids Relat. Interdiscip. Top.*, vol. 63, pp. 046 604/1–046 604/13, Mar. 2001.

[8] P. Markos and C. M. Soukoulis, "Transmission studies of left-handed materials," *Phys. Rev. B, Condens Matter.*, vol. 65, pp. 033 401/1–033 401/4, Dec. 2001.

[9] M. Bayindir, K. Aydin, and E. Ozbay, "Transmission properties of composite metamaterials in free space," *App. Phys Lett.*, vol. 81, no. 1, pp. 120–122, July 2002.

[10] R. Ruppin, "Surface polaritons of a left-handed medium," *J. Phys., Condens. Matter*, vol. 13, p. 1811, 2001.

[11] J. B. Pendry, A. J. Holden, D. J. Robbins, and W. J. Stewart, "Magnetism from conductors and enhanced nonlinear phenomena," *IEEE Trans. Microwave Theory Tech.*, vol. 47, pp. 2075–2084, Nov. 1999.

[12] D. R. Smith, W. J. Padilla, D. C. Vier, S. C. Nemat-Nasser, and S. Schultz, "Composite medium with simultaneously negative permeability and permittivity," *Phys. Rev. Lett.*, vol. 84, pp. 4184–4187, May 2000.

[13] R. A. Shelby, D. R. Smith, and S. Schultz, "Experimental verification of a negative refractive index of refraction," *Science*, vol. 292, pp. 77–79, Apr. 2001.

[14] A. K. Iyer and G. V. Eleftheriades, "Negative refractive index metamaterials supporting 2-D wave propagation," in *IEEE MTT-S Int. Microwave Symp. Dig.*, vol. 2, Seattle, WA, June 2–7, 2002, pp. 1067–1070.

[15] R. W. Ziolkowski, "Design, fabrication, and testing of double negative metamaterials," *IEEE Trans. Antennas Propagat.*, vol. 51, pp. 1516–1529, July 2003.

[16] D. M. Pozar, *Microwave Engineering*, 2nd ed. New York: Wiley, 1998, p. 211.

[17] G. V. Eleftheriades, A. K. Iyer, and P. C. Kremer, "Planar negative refractive index media using periodically *L–C* loaded transmission lines," *IEEE Trans. Microwave Theory Tech.*, vol. 50, pp. 2702–2712, Dec. 2002.

[18] A. Grbic and G. V. Eleftheriades, "A backward-wave antenna based on negative refractive index *L–C* networks," in *IEEE Int. Antennas and Propagation Symp. Dig.*, vol. 4, San Antonio, TX, June 15–21, 2002, pp. 340–343.

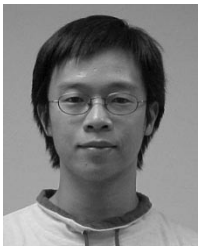

Ching-Ying Cheng (M'00) received the B.S.B.A degree in transportation management from Tamkang University, Taipei, Taiwan, R.O.C., in 1995, and the B.S. and M.S. degrees in electrical and computer engineering from the University of Arizona, Tucson, in 2001 and 2003, respectively.

From 1995 to 1997, he was a supervisor in the Taiwan Army. From 1999 to 2001, he was a Co-Op Engineer with Schott-Donnelly LLC, Tucson, AZ, where he performed multiple projects, including design and testing for low-power dc controllers utilizing electrochromic glass and participated in the development of RF transmitter/receiver systems. During Summer 2001, he was an Intern Engineer for Pulse Metric Inc., San Diego, CA, where he successfully designed and constructed test systems to verify the performance of cutting-edge medical equipment and where he completed their FDA requirements for attaining an on-schedule product release. From 2001 to 2003, he was a Research Assistant with the University of Arizona. His research interests focus on improving the performance of RF/microwave integrated circuits (ICs) and antennas using MTMs.

Mr. Cheng is a student member of the IEEE Antennas and Propagation Society (IEEE AP-S).

Richard W. Ziolkowski (M'87–SM'91–F'94) received the Sc.B. degree in physics (*magna cum laude*) (with honors) from Brown University, Providence, RI, in 1974, and the M.S. and Ph.D. degrees in physics from the University of Illinois at Urbana-Champaign, in 1975 and 1980, respectively.

From 1981 to 1990, he was a member of the Engineering Research Division, Lawrence Livermore National Laboratory. From 1984 to 1990, he served as the Leader of the Computational Electronics and Electromagnetics Thrust Area for the Engineering Directorate. In 1990, he joined the Department of Electrical and Computer Engineering, University of Arizona, Tucson, as an Associate Professor. In 1996, he was became a Full Professor. His research interests include the application of new mathematical and numerical methods to linear and nonlinear problems dealing with the interaction of acoustic and electromagnetic waves with complex media, MTMs, and realistic structures. For the Optical Society of America (OSA), he was a co-guest editor of the 1998 Special Issue of the *Journal of the Optical Society of America A*, which featured mathematics and modeling in modern optics.

Prof. Ziolkowski is a member of Tau Beta Pi, Sigma Xi, Phi Kappa Phi, the American Physical Society, the Optical Society of America, the Acoustical Society of America, and Commissions B (Fields and Waves) and D (Electronics and Photonics) of the International Union of Radio Science (URSI). He was an associate editor for the IEEE TRANSACTIONS ON ANTENNAS AND PROPAGATION (1993–1998). He served as the vice chairman of the 1989 IEEE Antennas and Propagation Society (IEEE AP-S) and URSI Symposium in San Jose, CA, and as the Technical Program chairperson for the 1998 IEEE Conference on Electromagnetic Field Computation, Tucson, AZ. He served as a member of the IEEE AP-S Administrative Committee (AdCom) (2000–2002). He was a co-guest editor for the IEEE TRANSACTIONS ON ANTENNAS AND PROPAGATION Special Issue on Metamaterials in 2003. For the U.S. URSI Society, he served as secretary for Commission B (Fields and Waves) (1993–1996) and as chairperson of the Technical Activities committee (1997–1999), and as secretary for Commission D (Electronics and Photonics) (2001–2002). He served as a member-at-large of the U.S. National Committee (USNC) of URSI (2000–2002) and is currently a member of the International Commission B Technical Activities Board. He was a co-organizer of the Photonics Nanostructures Special Symposia at the 1998–2000 OSA Integrated Photonics Research (IPR) Topical Meetings. He served as the chair of the IPR Sub-Committee IV, Nanostructure Photonics, in 2001. He was the recipient of the 1993 Tau Beta Pi Professor of the Year Award and the 1993 and 1998 IEEE and Eta Kappa Nu Outstanding Teaching Award.